

Platinum Nanoparticle Loading of Boron Nitride Aerogel and Its Use as a Novel Material for Low-Power Catalytic Gas Sensing

Anna Harley-Trochimczyk, Thang Pham, Jiyoung Chang, Ernest Chen, Marcus A. Worsley, Alex Zettl, William Mickelson, and Roya Maboudian*

A high-surface-area, highly crystalline boron nitride aerogel synthesized with nonhazardous reactants has been loaded with crystalline platinum nanoparticles to form a novel nanomaterial that exhibits many advantages for use in a catalytic gas sensing application. The platinum nanoparticle-loaded boron nitride aerogel integrated onto a microheater platform allows for calorimetric propane detection. The boron nitride aerogel exhibits thermal stability up to 900 °C and supports disperse platinum nanoparticles, with no sintering observed after 24 h of high-temperature testing. The high thermal conductivity and low density of the boron nitride aerogel result in an order of magnitude faster response and recovery times (<2 s) than reported on alumina support and allow for 10% duty cycling of the microheater with no loss in sensitivity. The resulting 1.5 mW sensor power consumption is two orders of magnitude less than commercially available catalytic gas sensors and unlocks the potential for wireless, battery-powered catalytic gas sensing.

1. Introduction

Hexagonal boron nitride (h-BN) is a 2D material that has generated great interest due to its unique optical, electrical, and thermal properties.^[1–3] While structurally similar to graphite and graphene, h-BN has a distinct set of complementary and, in many cases, advantageous properties compared to its

carbon analogs. For example, h-BN is a wide band gap insulator (independent of morphology), yet has high thermal conductivity, high resistance to oxidation, and the lowest density among non-oxide ceramics.^[4–6] Having a similar sp²-bonding configuration to graphite, h-BN can be synthesized in analogous lower dimensional forms, such as nanotubes (1D)^[7,8] and nanosheets (2D),^[9,10] which have high specific surface area, among their other qualities. To exploit the high surface area of these nanomaterials in a 3D geometry, there have been efforts to synthesize low density, high surface area 3D structures of BN comprised of lower dimensional nanomaterials.^[11–14] These high surface area 3D BN materials have been proposed for hydrogen storage,^[15–18] hydrocarbon uptake,^[19–21] and water purification^[17,22]

due to the enhanced physisorption properties of BN compared to carbon.^[23] In addition to these applications, high surface area BN is an interesting candidate as a support material for optically or catalytically active nanoparticles, due to its wide band gap and chemical inertness. Nanoparticle-loaded boron nitride has been studied for use in high temperature or harsh environment catalytic applications in gas^[24–27] and liquid phases.^[28] In these previous catalysis-focused works, the porous BN is of varying crystallinity and specific surface area, and many of the synthesis processes for the porous BN and the nanoparticle decoration rely on hazardous liquid precursors and reducing species. Recently, a novel method for the synthesis of highly crystalline, high specific surface area, sp²-bonded boron nitride aerogels using nonhazardous reactants has been developed.^[11] In this paper, we report the loading of this highly crystalline, high surface area, mesoporous boron nitride aerogel with well-dispersed platinum nanoparticles, and as an example of its utility, we demonstrate low-power, fast, and sensitive catalytic gas sensing.

To assess the catalytic activity and stability of the Pt nanoparticle-loaded boron nitride aerogel (Pt-BN) presented here, the aerogel is integrated onto a microheater to form a catalytic gas sensor or micropellistor. Low-power catalytic gas sensors are in demand for fast leak detection in hydrogen and hydrocarbon generation, handling, storage, and transport. Early warning of leaks will result in increased safety

A. Harley-Trochimczyk, E. Chen, Dr. W. Mickelson,
Prof. R. Maboudian
Department of Chemical and Biomolecular Engineering
University of California at Berkeley
Berkeley, CA 94720, USA
E-mail: maboudia@berkeley.edu

T. Pham, Dr. J. Chang, Prof. A. Zettl
Department of Physics
University of California at Berkeley
Materials Sciences Division
Lawrence Berkeley National Laboratory
Kavli Energy NanoSciences Institute at the University of California at
Berkeley and The Lawrence Berkeley National Laboratory
Berkeley, CA 94720, USA

Dr. M. A. Worsley
Physical and Life Science Directorate
Lawrence Livermore National Laboratory
7000 East Avenue, Livermore, CA 94550, USA



DOI: 10.1002/adfm.201503605

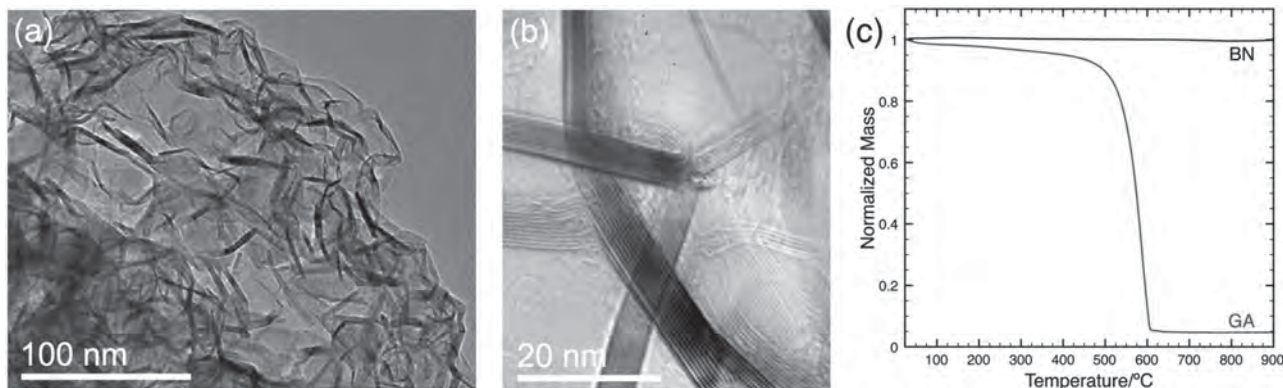


Figure 1. a) TEM of bare boron nitride aerogel. b) High resolution TEM of boron nitride aerogel showing highly crystalline, few layer BN. c) TGA of boron nitride aerogel^[21] and graphene aerogel (GA),^[37] showing improved thermal stability of the BN aerogel.

and environmental protection. Research efforts have focused on porous alumina supports,^[29–31] which suffer from low thermal conductivity, and thin films of catalytic metals,^[30,32–34] which have low active surface area. Boron nitride aerogel offers enhanced thermal conductivity compared to alumina, and a high surface area for increased nanoparticle loading in a constrained volume of the microfabricated sensor. Increased thermal conductivity of the support allows heat generated during gas combustion to be efficiently transferred to the microheater and raise its temperature. Catalytic gas sensing using the newly developed Pt-BN demonstrates the advantage of this material.

2. Results and Discussion

2.1. Synthesis and Characterization of Platinum-Loaded Boron Nitride Aerogel

Boron nitride aerogel acts as an ideal catalyst support due to its high specific surface area, good thermal stability, and high thermal conductivity. BN aerogel synthesis follows the procedure of Rousseas et al.^[11] where graphene aerogel (GA) is converted to boron nitride aerogel through the carbothermic reduction of boron oxide and concurrent nitridation with nitrogen gas. The resulting few layer sp^2 -bonded BN maintains the microporous structure of the graphene aerogel and has a high specific surface area ($\approx 500 \text{ m}^2 \text{ g}^{-1}$). The high specific surface area allows, in principle, for high catalyst nanoparticle loading while minimizing the mass of the catalyst support. Furthermore, BN exhibits a high resistance to oxidation at elevated temperature,^[1] which is paramount to robust long-term operation in high temperature catalysis applications. The synthesized BN aerogel also maintains a high degree of crystallinity imparted by the graphene aerogel, and in fact, the degree of crystallinity may increase during the conversion process.^[11] The highly crystalline aerogel allows the thermal conductivity of the h-BN to be preserved better than a porous BN structure with less order. Hexagonal BN has high thermal conductivity ($\approx 250 \text{ W m}^{-1} \text{ K}^{-1}$),^[6] especially compared to alumina, the most common catalyst support ($\approx 10 \text{ W m}^{-1} \text{ K}^{-1}$).^[35] The thermal conductivity of the BN aerogel allows heat generated during

exothermic reactions to be more effectively dissipated. Without this heat dissipation, hot spots can build up and cause sintering of the catalytic nanoparticles or damage to the support itself.

The as-synthesized BN aerogel can be seen in **Figure 1a** with a transmission electron microscopy (TEM) image showing the wrinkled BN sheets displaying features on the tens of nanometers scale. As seen in the high-resolution TEM image in **Figure 1b**, the aerogel is comprised of highly crystalline few-layer BN. The junctions between BN sheets within the aerogel are comprised of covalent bonds, which lead to improved thermal conductivity compared to randomly stacked BN sheets.^[36] Thermogravimetric analysis (TGA) of the boron nitride aerogel compared to the graphene aerogel starting material^[37] shows the improved thermal stability, with graphene aerogel showing a 50% loss in mass by 575 °C, while the boron nitride aerogel has <1% change in mass during heating up to 900 °C (**Figure 1c**).

Noble metals, especially platinum and palladium, have been widely used for catalysis, especially oxidation reactions that require high temperatures for appreciable reaction rates.^[38] Platinum nanoparticle size, crystallinity, and interaction with the support all affect catalytic activity. In this paper, platinum catalyst loading of the BN aerogel is achieved by immersing the aerogel in chloroplatinic acid in ethanol, drying, and annealing in argon at high temperature to form crystalline platinum nanoparticles (Experimental Section). Optical images of the boron nitride aerogel before and after platinum loading can be found in **Figure S1** (Supporting Information). From measurement of the aerogel weight before and after platinum loading, a platinum weight ratio of 45% is calculated. Specific surface area of the platinum nanoparticle-loaded boron nitride aerogel is $275 \text{ m}^2 \text{ g}^{-1}$. The decrease in the specific surface area from the bare aerogel is expected since the high loading of platinum increases the weight without significantly changing the surface area. Scanning electron microscopy (SEM) images of the Pt-BN show that the porosity and high surface area of the aerogel, as seen by TEM, are representative of the entire aerogel structure and are not diminished after the nanoparticle loading process (**Figure 2a**). In **Figure 2b**, a TEM image of the platinum nanoparticle-loaded boron nitride aerogel confirms the presence of crystalline nanoparticles with average diameter of $17 \text{ nm} \pm 6 \text{ nm}$, based on 150 particles (distribution of particle

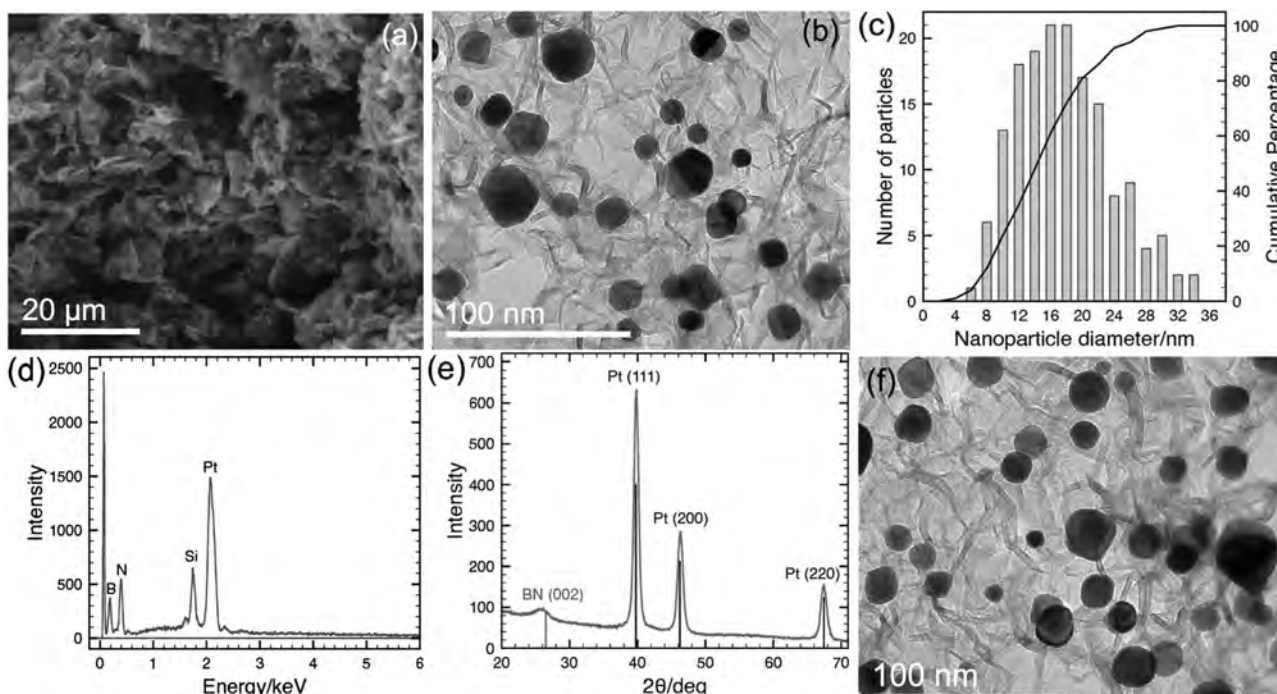


Figure 2. a) SEM of BN aerogel after Pt nanoparticle loading showing retained porosity and high surface area. b) TEM of BN aerogel after Pt nanoparticle loading. c) Size distribution of platinum nanoparticles. d) EDAX results confirming presence of B, N, and Pt. e) XRD spectra showing BN (002) peak and Pt (111), (200), and (220) peaks. f) TEM image of Pt-BN after heating in open-air furnace for 24 h at 500 °C shows no sintering or aggregation of platinum nanoparticles.

size shown in Figure 2c). Additional TEM images used for particle analysis can be found in Figure S2 (Supporting Information).

To determine the chemical composition and physical structure of the nanoparticles, energy dispersive X-ray spectroscopy (EDAX) and X-ray diffraction (XRD) are performed. The EDAX spectra in Figure 2d confirms the presence of Pt, as well as B and N (the Si peak is from the sample substrate) with no detectible amount of chlorine, suggesting that the platinum salt has been completely reduced to elemental platinum. No presence of carbon is detected in the EDAX measurements, suggesting complete conversion of the graphene aerogel in the formation of the BN aerogel. The presence of metallic platinum is further confirmed via XRD in Figure 2e, which shows the characteristic (111), (200), and (220) peaks of the Pt face-centered cubic structure, as well as the BN (002) peak. The crystalline nature of the platinum nanoparticles is also evident in the faceted shapes observed in the TEM images. The relatively low intensity of the BN (002) peak in the XRD spectra results from the high loading of platinum and the low density of the BN aerogel.

Interaction between the Pt nanoparticles and the BN support is important for maintaining nanoparticle dispersion, especially during high temperature operation. The Pt-BN reported here maintains good stability of the nanoparticle size and dispersion after heating in air at 500 °C for 24 h, as shown in Figure 2f. No measurable platinum nanoparticle sintering is observed. Analysis of platinum nanoparticle size and size distribution leads to an average particle size of $17.6 \text{ nm} \pm 5 \text{ nm}$, which is not statistically different from the Pt-BN before heating (nanoparticle size distribution and additional TEM images in Figure S3,

Supporting Information). Prior work has suggested that a high degree of BN crystallinity led to platinum aggregation at elevated temperature due to the weaker interaction of the crystal face of h-BN with Pt compared to the edges or defects.^[39] Despite having a high degree of crystallinity in the boron nitride aerogel reported here, the platinum remains well dispersed and tightly adhered. For the TEM analysis, the Pt-BN is sonicated in isopropyl alcohol for 30 min before dispensing on a lacey carbon grid. Despite this, the TEM images show high nanoparticle density on the BN sheets and no free Pt nanoparticles visible on the lacey carbon, indicating a strong interaction between the Pt nanoparticles and BN. Partial encapsulation of the nanoparticle within the pores of the BN aerogel or chemical stabilization from defects at the cross-linking sites within the aerogel may explain the improved platinum dispersion within the BN aerogel. The mesoporosity of the BN aerogel effectively prevents sintering of the platinum nanoparticles, allowing activity to be maintained even during high temperature operation.

2.2. Catalytic Gas Sensing Performance

Catalytic gas sensors are prepared by drop casting a suspension of Pt-BN (or BN) aerogel material onto a low-power microfabricated heater platform (Experimental Section). The microheater used in this work consists of a polycrystalline silicon (polysilicon) trace encapsulated in a thin silicon nitride membrane and can reach 500 °C with only 15 mW peak power. Details of the microheater fabrication and characterization have been published previously.^[40,41] The cross-sectional schematic of

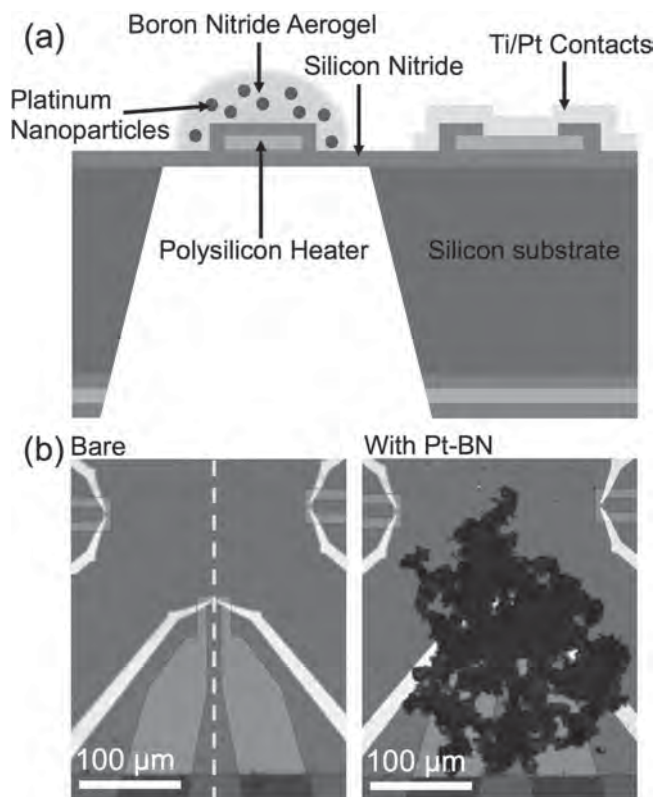


Figure 3. a) Schematic of sensor cross-section. Pt-BN is drop cast on top of microheater platform. When the sensor is exposed to catalytic gas, the gas reacts with oxygen on the surface of the platinum nanoparticles and releases heat, which increases the temperature and, correspondingly, the resistance of the polysilicon microheater. b) Optical images of one microheater before and after Pt-BN deposition. The dotted line on bare the microheater image indicates where cross-section in (a) would be located.

the fabricated sensor in **Figure 3a** and the optical images in **Figure 3b** show the Pt-BN deposited on the heater area of one microheater. Sensor testing is performed using propane gas as a representative combustible gas because it is a commonly used hydrocarbon in heating, cooking, power generation, oil

recovery,^[42,43] and even refrigeration.^[44,45] When the sensor is exposed to propane gas in air, combustion of propane on the surface of the platinum nanoparticles releases heat, which increases the temperature and the resistance of the polysilicon microheater, since it has a positive thermal coefficient of resistance (TCR) (**Figure S4**, Supporting Information). Sensor response is reported as $(R - R_0)/R_0 \times 100\%$, where R_0 is the average resistance in air and R is the average resistance during exposure to a given concentration of propane. Sensor testing is performed in synthetic air to control the oxygen concentration. A microheater operating temperature of 500 °C gives the best sensitivity while remaining in the linear TCR window of the polysilicon. Because the lower explosive limit of propane in air is 21 000 ppm or 2.1%,^[46] tests are performed with gas concentrations from 5000 to 20 000 ppm. Sensor tests performed with bare BN showed no response to propane.

The low density and high thermal conductivity of BN enables superior catalytic gas sensing performance in terms of response and recovery time and sensor power consumption. The Pt-BN sensor resistance over time shown in **Figure 4a** exhibits low noise and fast response and recovery through range of propane concentrations tested. Because boron nitride has a high thermal conductivity, heat generated during propane combustion can be efficiently transferred to the microheater and raise its temperature. Additionally, the low density and high surface area means a minimized mass of the support material within a given volume so less of the heat generated in the exothermic reaction will go to heating the support. Graphene aerogel has similar advantages of surface area and thermal conductivity and performs well for hydrogen sensing,^[40] but methane and other lower alkanes require higher catalyst temperatures for detection (≈ 500 °C), which is above the long-term thermal stability range for graphene aerogel (see **Figure 1c**). Closer analysis of the data in **Figure 4a** shows the average time to reach 90% of the full sensor response (t_{90}) is only 1.35 s for the response and 0.6 s for the recovery (**Figure 4b** shows a closer view of the response and recovery for 15 000 ppm as a sample). In comparison, commercial products and reports from literature using a porous alumina support have shown response times from 10 to 20 s.^[30,47] The sensor power consumption also benefits from this fast

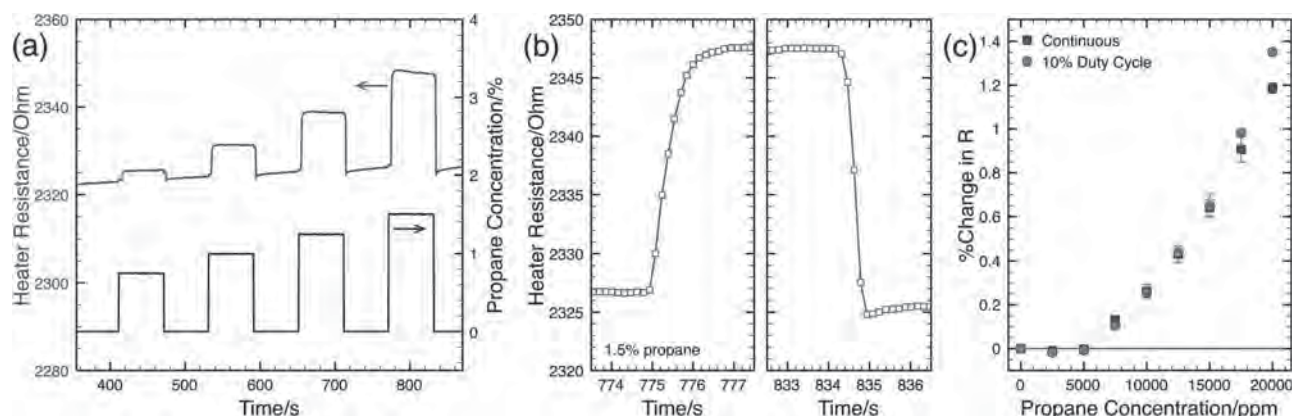


Figure 4. a) Pt-BN sensor resistance when exposed to varying propane concentrations showing stable, fast response. b) Sensor response (left) and recovery (right) shown in close up for 15 000 ppm propane exposure. c) Response of Pt-BN sensor versus propane concentration while heated to 500 °C continuously (squares) and for 100 ms every second (circles), which lowers the overall power consumption to only 1.5 mW.

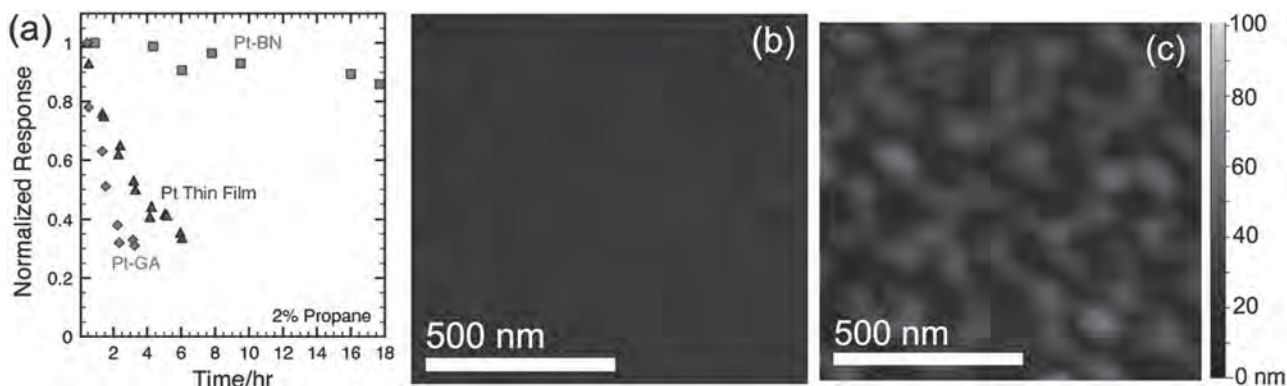


Figure 5. a) Normalized response to propane (2% or 20 000 ppm) versus time for Pt-BN sensors (squares), Pt-GA (diamonds), and an evaporated Pt thin film (triangles), showing the enhanced stability of Pt-BN sensor. AFM images of platinum thin film b) as evaporated (root mean square (RMS) roughness = 1.62 nm) and c) after 6 h of high temperature testing (RMS roughness = 12.18 nm) showing film agglomeration (Z-range of 100 nm in both images).

response and recovery, as it makes duty cycling of the microheater possible. Figure 4c shows the sensor response versus propane concentration for continuous heating and heating for 100 ms every second, thereby reducing the average power from 15 to 1.5 mW without compromising response magnitude or measurement frequency. Single mW power consumption represents a two order of magnitude reduction from commercially available catalytic gas sensors.^[48] Along with minimizing power requirements, cycling the microheater through various temperatures can also allow for selective measurement of combustible gases. Each combustible gas has a unique response curve over a range of temperatures and if this is well characterized for a set of gases in a mixture of interest, measurements collected from the catalytic gas sensor at various temperatures can be analyzed to give single component response.^[49]

Stable, reproducible sensor performance relies both on the stability of the boron nitride support and the platinum nanoparticles. Previous works using BN as a catalyst support have suggested that the high thermal conductivity of BN improves the catalyst lifetime by dissipating heat generated in oxidation reactions and preventing the buildup of hot spots that can cause serious nanoparticle sintering.^[26,50] As discussed with Figure 2f, high temperature treatment of the Pt-BN does not result in an increase in platinum nanoparticle size over 24 h at 500 °C. To determine whether this stable Pt nanoparticle size on the BN aerogel translates to more stable catalyst performance, Pt-BN sensors were tested for several hours and compared to sensors fabricated with other forms of Pt. **Figure 5a** shows the normalized response to 2% (20 000 ppm) propane of Pt-BN sensors compared to sensors made with platinum nanoparticle-loaded graphene aerogel (Pt-GA) and an evaporated Pt thin film. It is evident that the response of the Pt-BN sensor is significantly more stable than both the Pt-GA and the Pt thin film, with only a 14% decrease over 18 h of operation compared to a drop of 50% in 2–3 h for the other sensors. Atomic force microscopy (AFM) of the platinum thin film, shown in Figure 5b,c, reveals that the film undergoes agglomeration during high temperature testing. Optical analysis of the Pt-GA after 4 h of testing shows a loss of material that can be attributed to the graphene aerogel support burning off.^[51]

3. Conclusion

In summary, a high surface area, highly crystalline boron nitride aerogel synthesized with nonhazardous reactants has been loaded with crystalline platinum nanoparticles to form a novel nanomaterial that exhibits many advantages for use in a catalytic gas sensing application. Platinum nanoparticle-loaded boron nitride aerogel integrated onto a microheater platform allows for calorimetric propane detection. Boron nitride aerogel exhibits thermal stability up to 900 °C and supports disperse platinum nanoparticles, with no sintering observed after 24 h of high temperature testing. The high thermal conductivity and low density of the boron nitride aerogel results in an order of magnitude faster response and recovery times (<2 s) than reported on alumina support and allows for 10% duty cycling of the microheater with no loss in sensitivity. The resulting 1.5 mW sensor power consumption is two orders of magnitude less than commercially available catalytic gas sensors and unlocks the potential for wireless, battery-powered catalytic gas sensing. The approach presented in this paper can be extended to nanoparticle loading of metals other than platinum, allowing improved performance for other hydrocarbon sensing.

4. Experimental Section

Pt-BN Synthesis: Details of BN aerogel synthesis can be found Rousseas et al.^[11] In summary, graphene aerogel is converted to BN aerogel via carbothermic reduction in the presence of B₂O₃ vapor and N₂ gas at high temperature (1600–1800 °C). The as-synthesized BN aerogel was then infiltrated with solution of acid chloroplatinic (H₂PtCl₆) (Sigma Aldrich) and ethanol with concentration of 0.5 M. The sample was annealed in conventional tube furnace under Ar (50 sccm) at 600 °C for 2 h in order to thermally reduce the platinum complex to pure Pt metal.

Pt-BN Characterization: BN and Pt-BN aerogels were dispersed in isopropanol by sonication and then dropped cast onto lacey carbon grid for TEM characterization using JOEL 2010 microscope. SEM (FEI Sirion XL30) with elemental analysis capacity using EDAX was used to investigate the aerogel morphology and Pt loading. X-ray diffraction for elemental and structure analysis used an AXS D8 Discover General Area Detector Diffraction System from Bruker with radiation from a Cu target ($K\alpha$, $\lambda = 0.15406$ nm). Specific surface area was calculated from

the nitrogen adsorption isotherm using the Brunauer–Teller–Emmett method with a Micromeritics ASAP 2420 porosimeter.

Sensor Fabrication: Microheater fabrication is described in full by Harley-Trochimczyk et al.^[40] Briefly, a silicon substrate was coated with silicon-rich low-stress nitride (100 nm), followed by boron-doped polysilicon (100 nm), which was patterned to form the microheater. Another silicon nitride layer (100 nm) was deposited and windows were patterned for the microheater contacts, which were e-beam evaporated titanium/platinum (10/90 nm). The back side of the wafer was patterned and etched to expose the silicon substrate, which was etched in KOH to release the silicon nitride membrane. The Ti/Pt electrodes overlaid on the microheater, seen in Figure 3b, are not used in this sensor measurement and are not included in the cross-section in Figure 3a. One microheater chip (3.5 mm × 3.5 mm) is wire bonded into a 14-pin cer-dip package for electrical characterization and sensor testing. BN and Pt-BN aerogels were dispersed in isopropanol by sonication and drop cast (six drops of 0.6 μL each) onto the microheater chip while one of the microheaters was powered to 65 °C to promote solvent evaporation and material deposition at the center of the microheater.

Gas Sensing System: The sensor was placed in a gas flow chamber (1 mL volume). Gas exposure and signal collection were done using Labview and an open-source Java-based instrument and control and measurement software suite, Zephyr.^[52] Gas tanks of pure nitrogen, pure oxygen, and 5% propane balanced in nitrogen (Praxair) were controlled with mass flow controllers (Bronkhurst) and mixed to give the desired oxygen (21%) and propane concentrations (0%–2%) with a total flow rate of 300 sccm. For sensor signal collection, a bias voltage was applied to the microheater and the microheater resistance was measured with a Keithley 2602 source-meter.

Pt Thin Film Fabrication and Characterization: Silicon dioxide (20 nm) and platinum (6 nm) were thermally evaporated (Thermionics VE-100 Vacuum Evaporator) onto the microheater chip with one set of wire-bond pads physically masked. The silicon dioxide prevented the platinum thin film from creating a shorting path between microheater contacts. The microheater was wire bonded into the cer-dip package and tested in the gas sensing system described above. After testing, the microheater chip was removed from the cer-dip package and atomic force microscopy was performed (Digital Instruments NanoScope IIIa, tapping mode) to characterize the agglomeration of the film.

Supporting Information

Supporting Information is available from the Wiley Online Library or from the author.

Acknowledgements

The authors would like to thank Hu Long for his assistance with the XRD measurements, Dr. Qin Zhou for help with microheater fabrication, and Kristen Colwell for her assistance with the surface area measurements. The authors gratefully acknowledge funding from the National Science Foundation (NSF), including the NSF Innovation Corps program (Award No. 1357682) and NSF Acceleration Innovation Research: Technology Transfer program (IIP 1444950), and from the UC Lab Fees Research Program under award 12-LR-235323 which provided for graphene aerogel synthesis. Devices were partially fabricated at the Marvell Nanofabrication Facility on the UC Berkeley campus. XRD was done at the Molecular Foundry and supported by the Office of Science, Office of Basic Energy Sciences, of the U.S. Department of Energy under Contract No. DE-AC02-05CH11231. A.H.-T. acknowledges additional support through the National Science Foundation Graduate Research Fellowship under Grant No. DGE 1106400. A.Z., T.P., and J.C. received support from the Director, Office of Basic Energy Sciences, Materials Sciences and Engineering Division, of the U.S. Department of Energy under Contract No. DE-AC02-05CH11231, which provided for student and postdoctoral support, and TEM and SEM characterization. A.Z. and M.W. received

additional support from the Air Force Office of Scientific Research under grant FA9550-14-1-0323, which provided for synthesis of the BN aerogels.

Received: August 26, 2015

Revised: October 7, 2015

Published online:

- [1] Y. Chen, J. Zou, S. J. Campbell, G. Le Caer, *Appl. Phys. Lett.* **2004**, *84*, 2430.
- [2] C. G. Cofer, J. Economy, *Carbon* **1995**, *33*, 389.
- [3] L. H. Li, J. Cervinka, K. Watanabe, T. Taniguchi, Y. Chen, *ACS Nano* **2014**, *8*, 1457.
- [4] M. L. Cohen, A. Zettl, *Phys. Today* **2010**, *63*, 34.
- [5] S. Bernard, P. Miele, *Mater. Today* **2014**, *17*, 443.
- [6] I. Jo, M. T. Pettes, J. Kim, K. Watanabe, T. Taniguchi, Z. Yao, L. Shi, *Nano Lett.* **2013**, *13*, 550.
- [7] N. G. Chopra, R. J. Luyken, K. Cherrey, V. H. Crespi, M. L. Cohen, S. G. Louie, A. Zettl, *Science* **1995**, *269*, 966.
- [8] D. Golberg, Y. Bando, C. Tang, C. Zhi, *Adv. Mater.* **2007**, *19*, 2413.
- [9] D. Golberg, Y. Bando, Y. Huang, T. Terao, M. Mitome, C. Tang, C. Zhi, *ACS Nano* **2010**, *4*, 2979.
- [10] G. R. Bhimanapati, D. Kozuch, J. Robinson, *Nanoscale* **2014**, *6*, 11671.
- [11] M. Rousseas, A. P. Goldstein, W. Mickelson, M. A. Worsley, L. Woo, A. Zettl, *ACS Nano* **2013**, *7*, 8540.
- [12] X. Huang, C. Tan, Z. Yin, H. Zhang, *Adv. Mater.* **2014**, *26*, 2185.
- [13] Y. Song, B. Li, S. Yang, G. Ding, C. Zhang, X. Xie, *Sci. Rep.* **2015**, *5*, 10337.
- [14] X. Zeng, L. Ye, S. Yu, R. Sun, J. Xu, C.-P. Wong, *Chem. Mater.* **2015**, *27*, 5849.
- [15] T. T. Borek, W. Ackerman, D. W. Hua, R. T. Paine, D. M. Smith, *Langmuir* **1991**, *7*, 2844.
- [16] Q. Wang, X. Wang, Y. Bando, D. Golberg, *Adv. Energy Mater.* **2014**, *4*, 1301525.
- [17] J. Li, J. Lin, X. Xu, X. Zhang, Y. Xue, J. Mi, Z. Mo, Y. Fan, L. Hu, X. Yang, J. Zhang, F. Meng, S. Yuan, C. Tang, *Nanotechnology* **2013**, *24*, 155603.
- [18] J. Kim, J. Han, M. Seo, S. Kang, D. Kim, J. Ihm, *J. Mater. Chem. A* **2013**, *1*, 1014.
- [19] W. Lei, D. Portehault, D. Liu, S. Qin, Y. Chen, *Nat. Commun.* **2013**, *4*, 1777.
- [20] Y. Zhang, L. Xu, B. Tang, Z. Li, *Catal. Sci. Technol.* **2013**, *3*, 222.
- [21] T. Pham, A. P. Goldstein, J. P. Lewicki, S. O. Kucheyev, C. Wang, T. P. Russell, M. A. Worsley, L. Woo, W. Mickelson, A. Zettl, *Nanoscale* **2015**, *7*, 10449.
- [22] F. Liu, J. Yu, X. Ji, M. Qian, *ACS Appl. Mater. Interfaces* **2015**, *7*, 1824.
- [23] S.-H. Jhi, Y.-K. Kwon, *Phys. Rev. B: Condens. Matter Mater. Phys.* **2004**, *69*, 245407.
- [24] J. A. Perdigón-Melón, A. Auroux, J. M. Guil, B. Bonnetot, *Stud. Surf. Sci. Catal.* **2002**, *143*, 227.
- [25] J. C.-S. Wu, C.-Y. Chen, S. D. Lin, *Catal. Lett.* **2005**, *102*, 223.
- [26] G. Postole, A. Gervasini, A. Auroux, B. Bonnetot, *Mater. Sci. Forum* **2006**, *518*, 203.
- [27] Y. Yabe, Y. Sawama, T. Yamada, S. Nagata, Y. Monguchi, H. Sajiki, *ChemCatChem* **2013**, *5*, 2360.
- [28] N. Meyer, K. Bekaert, D. Pirson, M. Devillers, S. Hermans, *Catal. Commun.* **2012**, *29*, 170.
- [29] L. Xu, Y. Wang, H. Zhou, Y. Liu, T. Li, Y. Wang, *J. Microelectromech. Syst.* **2012**, *21*, 1402.
- [30] I. Bárony, M. Ádám, P. Fürjes, R. Lucklum, M. Hirschfelder, S. Kulinyi, C. Dücső, *Meas. Sci. Technol.* **2009**, *20*, 124009.

- [31] P. Fürjes, M. Ádám, C. Dücsó, J. Zettner, I. Bársony, *Sens. Actuators, B* **2005**, 111–112, 96.
- [32] E. Vereshchagina, R. A. M. Wolters, J. G. E. Gardeniers, *Sens. Actuators, A* **2011**, 169, 308.
- [33] M. Zanini, J. H. Visser, L. Rimai, R. E. Soltis, A. Kovalchuk, D. W. Hoffman, E. M. Logothetis, U. Bonne, L. Brewer, O. W. Bynum, M. A. Richard, *Sens. Actuators, A* **1995**, 48, 187.
- [34] E. Karpov, E. F. Karpov, A. Suchkov, S. Mironov, A. Baranov, V. Sleptsov, L. Calliari, *Sens. Actuators, A* **2013**, 194, 176.
- [35] J. Small, J. Kushmerick, *Ceramics WebBook*, Sintered Alumina, National Institute of Standards and Technology, Gaithersburg, MD, USA **2001**.
- [36] S. M. Jung, H. Y. Jung, M. S. Dresselhaus, Y. J. Jung, J. Kong, *Sci. Rep.* **2012**, 2, 849.
- [37] M. A. Worsley, T. Pham, A. Yan, S. J. Shin, J. R. I. Lee, M. Bagge-Hansen, W. Mickelson, A. Zettl, *ACS Nano* **2014**, 8, 11013.
- [38] P. Gélín, M. Primet, *Appl. Catal., B* **2002**, 39, 1.
- [39] C.-A. Lin, J. C.-S. Wu, J.-W. Pan, C.-T. Yeh, *J. Catal.* **2002**, 210, 39.
- [40] A. Harley-Trochimczyk, J. Chang, Q. Zhou, J. Dong, T. Pham, M. A. Worsley, R. Maboudian, A. Zettl, W. Mickelson, *Sens. Actuators, B* **2015**, 206, 399.
- [41] Q. Zhou, A. Sussman, J. Chang, J. Dong, A. Zettl, W. Mickelson, *Sens. Actuators, A* **2015**, 223, 67.
- [42] J. G. Bralla, *Handbook of Manufacturing Processes: How Products, Components and Materials Are Made*, Industrial Press, New York **2007**.
- [43] J. Speight, *Handbook of Industrial Hydrocarbon Processes*, Elsevier, Amsterdam **2011**.
- [44] R. W. James, J. F. Missenden, *Int. J. Refrig.* **1992**, 15, 95.
- [45] M. A. Alsaad, M. A. Hammad, *Appl. Therm. Eng.* **1998**, 18, 911.
- [46] D. P. Nolan, *Handbook of Fire and Explosion Protection Engineering*, 3rd ed., Elsevier, Amsterdam **2011**.
- [47] C. Dücsó, M. Ádám, P. Fürjes, M. Hirschfelder, S. Kulinyi, I. Bársony, *Sens. Actuators, B* **2003**, 95, 189.
- [48] SGX Sensortech, *VQ548MP Datasheet*. SGX Sensortech, Essex, UK **2014**, p. 1.
- [49] R. E. Cavicchi, G. E. Poirier, N. H. Tea, M. Afridi, D. Berning, A. Hefner, J. Suehle, M. Gaitan, S. Semancik, C. Montgomery, *Sens. Actuators, B* **2004**, 97, 22.
- [50] J. C.-S. Wu, Z.-A. Lin, J.-W. Pan, M.-H. Rei, *Appl. Catal., A* **2001**, 219, 117.
- [51] A. Harley-Trochimczyk, J. Chang, T. Pham, J. Dong, M. A. Worsley, A. Zettl, W. Mickelson, R. Maboudian, presented at Transducers 2015, Int. Conf. Solid-State Sensors, Actuators and Microsystems, Anchorage, AK, USA, June **2015**.
- [52] S. Skarupo, *Eval. Eng.* **2007**, 46, 44.